RSC Advances

PAPER

View Article Online
View Journal | View Issue

Cite this: *RSC Adv.*, 2016, **6**, 58069

Facile synthesis and application of multi-shelled SnO_2 hollow spheres in lithium ion battery†

Guanglei Wu,*[a] Hongjing Wu,[b] Kuikui Wang,[a] Chenhui Zheng,[b] Yiqun Wang[b] and Ailing Feng*[c]

Received 6th May 2016
Accepted 10th June 2016

DOI: 10.1039/c6ra11771f

www.rsc.org/advances

A simple template-free hydrothermal method has been developed to prepare multi-shelled SnO_2 hollow spheres with controlled interior texture. The interior texture and size of the multi-shelled SnO_2 hollow spheres were found to be strongly dependent on the carbon source, Sn salt precursor and molar ratio of G : M. The multi-shelled SnO_2 hollow spheres exhibit good electrochemical performance as the anode material in lithium ion batteries.

Introduction

Wide-band gap semiconducting tin oxide (SnO_2) is a functional material of great interest. It should be emphasized that the performance of SnO_2 in some applications may actually benefit from a properly designed SnO_2 micro-/nanostructure.[1,2] Recently, hollow structures have attracted considerable attention because of their improvable performance, such as large specific surface area, complicated inner cavity, and high structural stability. More and more synthetic methods have been reported to prepare SnO_2 hollow structures, including Ostwald ripening, differential diffusion (*i.e.*, kirkendall effect), removable templates, and chemically induced self-assembly.[3] Usually, only single-shelled hollow spheres are obtained by the above-mentioned approaches.

It will be intellectually stimulating and technologically important to determine whether a high-order design (*e.g.*, hollow core–shell particles) of the micro-/nanostructure could lead to functional improvements, while depending on a relatively simple and scalable preparation method. Template-assisted synthesis is currently the most common preparation method of complicated hollow micro-/nanostructures. Recently, Wang and co-workers[4–11] have successfully prepared the multiple-shell metal oxide hollow microspheres by using carbonaceous microsphere as a template. Lou and co-workers[12] have developed a new "penetration-solidification-annealing" strategy to realize the general synthesis of various mixed metal oxide multi-shelled hollow spheres. Zhang *et al.* have constructed multi-shelled ZnO core–shell structures *via* a simple hard template strategy.[13] However, template-assisted synthesis is not without problems: product deconstruction during the template removal process, the shortage of templates for generating complicated hollow structures, and multistep and costly operations.

By comparison, hydrothermal synthesis has remarkable advantages such as simple operations, low-cost, and scalable production. In the present contribution, we report a simple approach for preparation of nanocrystalline SnO_2 hollow spheres with a controlled number of shells by chemically induced self-assembly in the hydrothermal environment.[14–16] To form the multi-shelled SnO_2 nanostructure, we add metal salts directly to the carbonhydrate solutions in water, followed by a hydrothermal treatment. Upon calcination, hollow spheres of SnO_2 were obtained. To evaluate the electrochemical characteristics of this material, we tested the multi-shelled SnO_2 hollow spheres as lithium storage anodes for secondary Li batteries.

Experimental

Materials

The reagents including D-glucose, source, $Na_2SnO_3 \cdot 3H_2O$, $SnCl_4 \cdot 5H_2O$, and $SnCl_2 \cdot 2H_2O$ were all analytical grade in purity, and bought from Sinopharm Chemical Reagent Co., Ltd. Ultrapure water (Millipore Milli-Q grade) with a resistivity of 18.2 MΩ was used in all the experiments.

Synthesis of single-shelled SnO_2 hollow spheres

In a typical experiment, 0.01 mol D-glucose and 0.02 mol Sn salt (*i.e.*, $Na_2SnO_3 \cdot 3H_2O$ and $SnCl_2 \cdot 2H_2O$) were dissolved in 50 ml ultrapure water. Then, the solution was homogenized by vigorous stirring. After stirring for 30 min, the resultant mixture was transferred to a 100 ml Teflon-lined autoclave followed by hydrothermal treatment at 180 °C for 20 h. The obtained

[a]*Institute of Materials for Energy and Environment, Growing Base for State Key Laboratory, College of Materials Science and Engineering, Qingdao University, Qingdao, 266071, P. R. China. E-mail: wuguanglei@mail.xjtu.edu.cn*

[b]*Department of Applied Physics, School of Science, Northwestern Polytechnical University, Xi'an, 710072, P. R. China*

[c]*Institute of Physics & Optoelectronics Technology, Baoji University of Arts and Sciences, Baoji 721016, P. R. China. E-mail: ailing@mail.xjtu.edu.cn*

† Electronic supplementary information (ESI) available. See DOI: 10.1039/c6ra11771f

products were washed and filtered off several times using ultrapure water and ethanol successively, and finally dried in a vacuum oven at 80 °C for 12 h. After synthesis, the products were subjected to annealing at 550 °C for 3 h in air with a heating rate of 2 °C min^{-1} from room temperature to obtain single-shelled SnO_2 hollow spheres.

Synthesis of multi-shelled SnO_2 hollow spheres

In a typical experiment, 0.0125 mol sucrose and 0.0125 mol Sn salt (*i.e.*, $SnCl_4 \cdot 5H_2O$) were dissolved in 50 ml ultrapure water. Alternatively, 0.02 mol D-glucose and 0.01 mol Sn salt (*i.e.*, $SnCl_4 \cdot 5H_2O$) were dissolved in 50 ml ultrapure water. Then, the solution was homogenized by vigorous stirring. After stirring for 30 min, the resultant mixture was transferred to a 100 ml Teflon-lined autoclave followed by hydrothermal treatment at 180 °C for 20 h. The obtained products were washed and filtered off several times using ultrapure water and ethanol successively, and finally dried in a vacuum oven at 80 °C for 12 h. After synthesis, the products were subjected to annealing at 500, 600 and 700 °C for 3 h in air with a heating rate of 2 °C min^{-1} from room temperature to obtain multi-shelled SnO_2 hollow spheres with controlled interior structures.

Characterization

The morphologies and structures of the as-prepared samples were visualized by using a FEI Quanta 600 FEG scanning electron microscope (SEM) and a FEI Tecnai G^2 F20 S-TWIN transmission electron microscope (TEM).

For evaluating the electrochemical performance of the materials, a mixture of 70 wt% SnO_2, 20 wt% acetylene black (AB) and 10 wt% polyvinylidene fluoride (PVDF) in *N*-methylpyrrolidone (NMP) solvent was taken as the slurry for casting. The slurry was

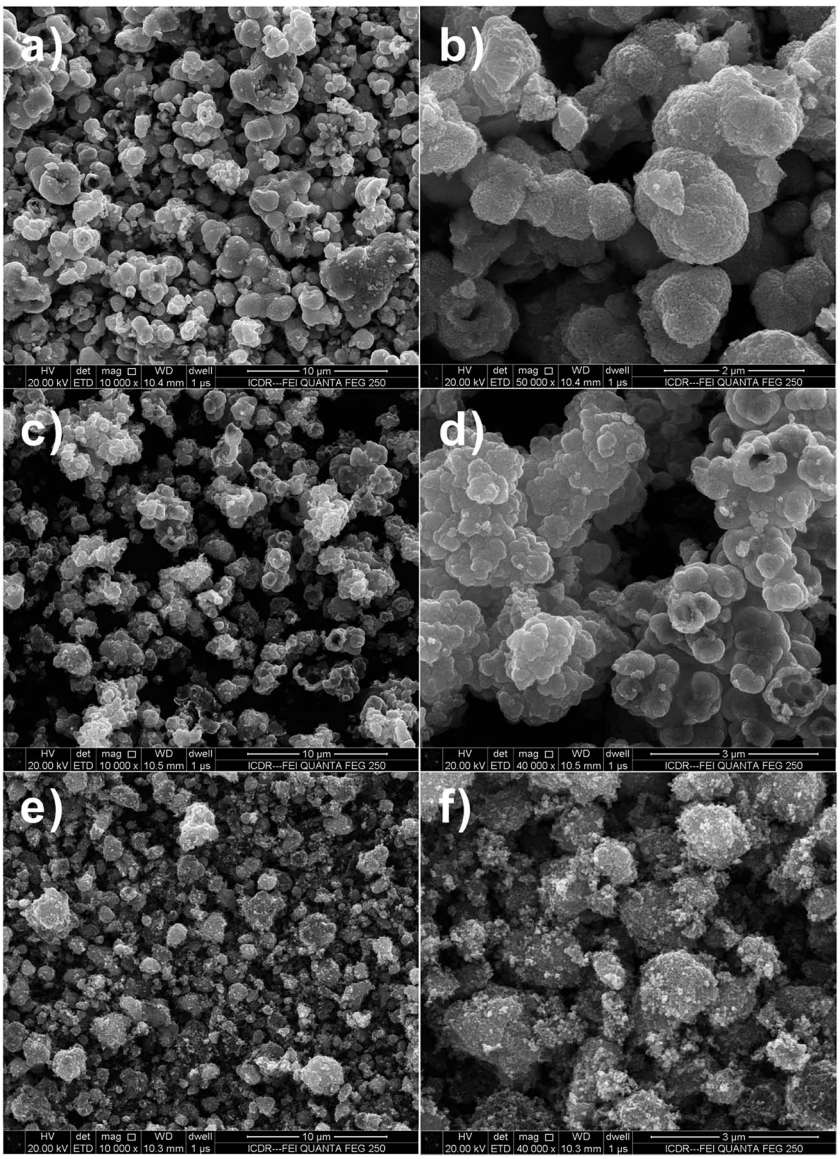

Fig. 1 FESEM images of SnO_2 samples after hydrothermal reaction at 180 °C with 1 : 2 molar ratio of D-glucose and metal salt. (a and b) $Na_2SnO_3 \cdot 3H_2O$, (c and d) $SnCl_2 \cdot 2H_2O$ and (e and f) $SnCl_4 \cdot 5H_2O$.

cast on the Cu foil followed by drying at 80 °C in a vacuum oven for 12 h. The electrochemical properties of the electrodes were measured by assembling them into coin cells (CR 2023) in an argon-filled glove box. Lithium foil was used as a counter electrode and a polypropylene (PP) film as the separator. The electrolyte was made from 1 M $LiPF_6$ in ethylene carbonate (EC) and diethyl carbonate (DEC) (1 : 1 by volume). The charging/discharging behavior of all the cells was galvanostatically cycled between 3 and 0.01 V. Capacity retention tests of the assembled cells were carried out for the required rates.

Results and discussion

Characterization of multi-shelled SnO_2 hollow spheres

The morphology and size of the SnO_2 hollow micro-/nanostructures were found to be strongly dependent on the Sn salt precursor. From the field-emission scanning electron microscopy (FESEM) image (Fig. 1a–d), it is apparent that the SnO_2 products prepared by using Na_2SnO_3 and $SnCl_2$ precursors consist of interconnected spherical hollow particles with a diameter in the range of 1–2 μm and shell thickness of about 100–200 nm. It was found that the salt precursor has a dramatic effect on both morphology and size of the product in present hydrothermal synthesis. For example, when the salt precursor was $SnCl_4$, the product consisted of irregular nanoparticles with a size in the range of 1–2 μm (Fig. 1e and f).

SnO_2 spheres are not solid ball but hollow sphere structures, as evidenced by the FESEM images of the products calcined at 550 °C in Fig. 2a–d. Observation on the surface of the product prepared by using $SnCl_4$ precursor, it is found that the calcined SnO_2 powder is made up from nano-sized small particles (Fig. 2e and f).

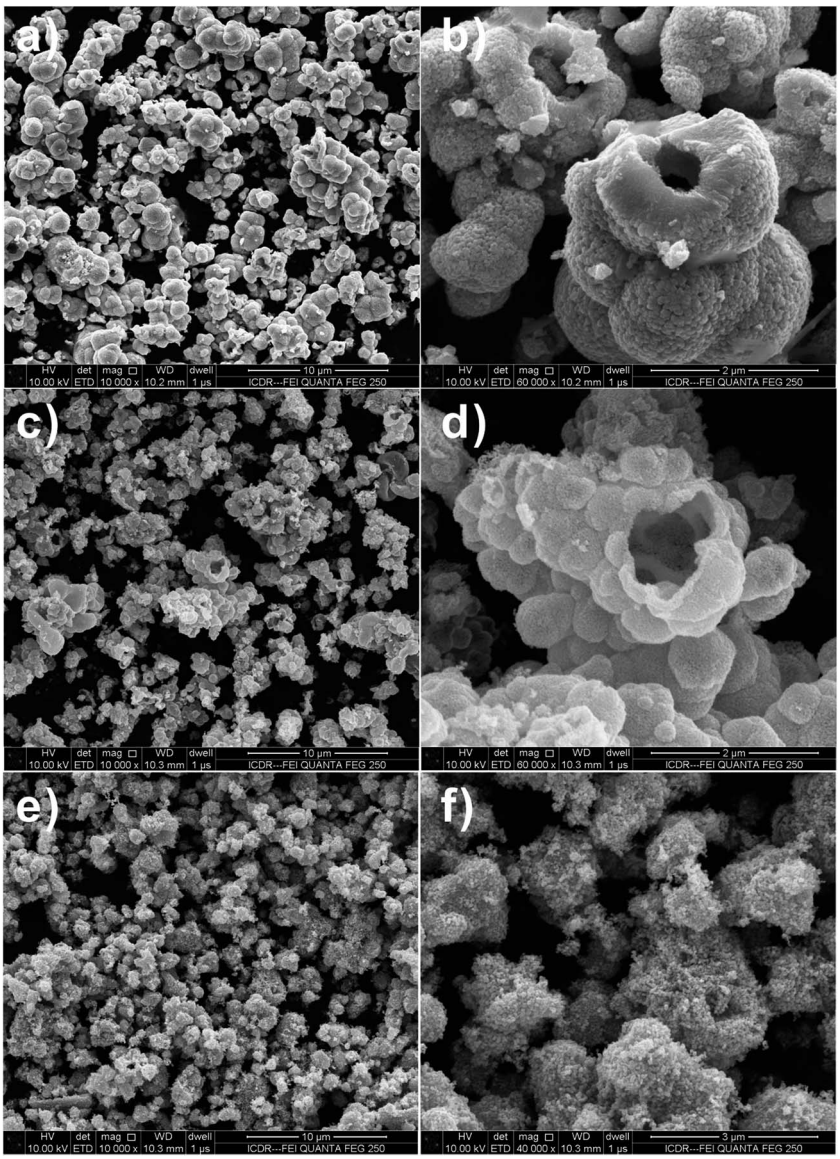

Fig. 2 FESEM images of SnO_2 samples after calcination at 550 °C for 3 h with 1 : 2 molar ratio of D-glucose and metal salt. (a and b) $Na_2SnO_3 \cdot 3H_2O$, (c and d) $SnCl_2 \cdot 2H_2O$ and (e and f) $SnCl_4 \cdot 5H_2O$.

Fig. 3a–f are FESEM images of the SnO_2 products with different proportions (*i.e.*, molar ratio of 1 : 0.4) of D-glucose (G) and Sn salt precursor (M) after calcination. It is found that only solid SnO_2 spheres exist in the final products, as the rate of hydrolysis of Sn ion is not as fast as that of carbonization of D-glucose, and thus the produced SnO_2 nanoparticle-loaded carbon spheres are formed.[17] All-solid spheres of SnO_2 nanoparticle aggregates are attributed to the uniformity of dispersion of SnO_2 nanoparticles in the carbon spheres. The irregular morphology of the SnO_2 nanoparticle aggregates (Fig. 3e and f) actually attested to the presence of a large number of SnO_2 nanoparticles surrounded by the amorphous carbon.

The high-magnification transmission electron microscopy (TEM) image in Fig. 4a shows hollow spheres, which has visibly hollow interiors and a coarse surface. TEM image of the surface morphology of SnO_2 spheres is shown as Fig. 4b, from which it can be clearly distinguished that the relatively large mesospheres comprises aggregates of fine particles with sizes of *ca.* 20 nm. The lattice fringe can be easily observed, and the lattice spacing (0.33 nm) agrees with SnO_2 (110) plane spacing from Fig. 4b.

The interior texture and size of the multi-shelled SnO_2 hollow spheres were found to be strongly dependent on the carbon source, Sn salt precursor and molar ratio of G : M. Fig. 5a, b, e and f show the FESEM images of the SnO_2 hollow spheres prepared by using $SnCl_4$ and $SnCl_2$ as the Sn salt precursors, sucrose as carbon source. The Sn source has important influence on the texture of the SnO_2 core–shell nanostructures. The morphology of the multi-shelled SnO_2 hollow spheres prepared by using $SnCl_4$ as the Sn source is revealed by FESEM observation (Fig. 5a and b). However, only single-shelled SnO_2 hollow spheres could be obtained by using

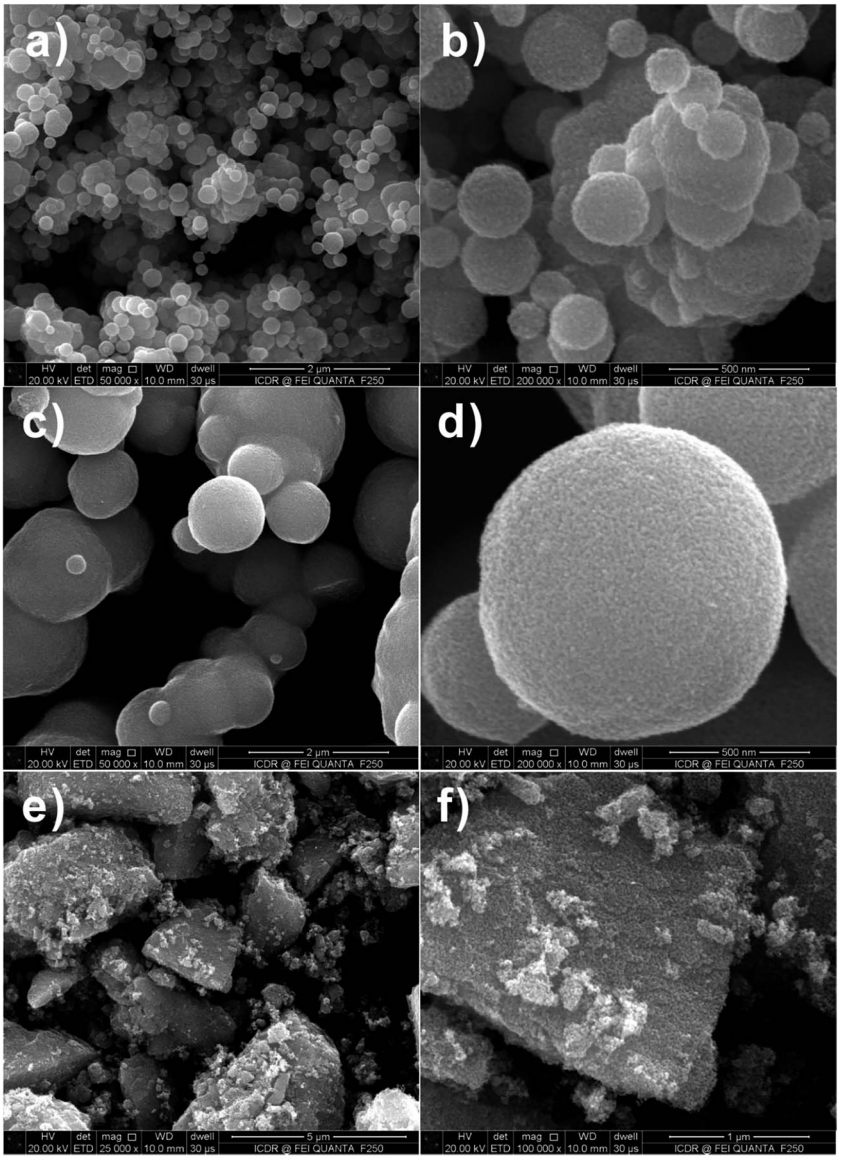

Fig. 3 FESEM images of SnO_2 samples after calcination at 550 °C for 3 h with 1 : 0.4 molar ratio of D-glucose and metal salt. (a and b) $Na_2SnO_3 \cdot 3H_2O$, (c and d) $SnCl_2 \cdot 2H_2O$ and (e and f) $SnCl_4 \cdot 5H_2O$.

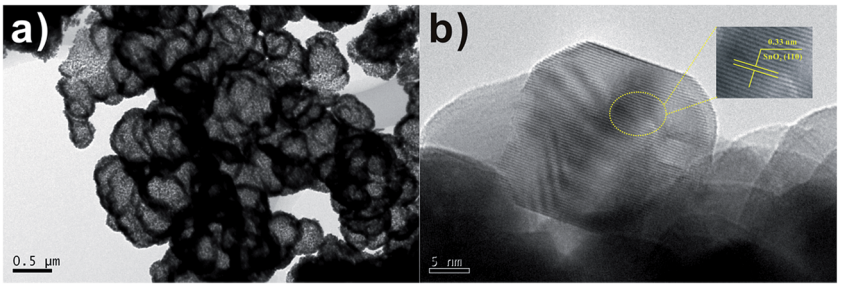

Fig. 4 (a) TEM (b) HRTEM images of SnO_2 samples after calcination at 550 °C for 3 h with 1 : 2 molar ratio of D-glucose and $SnCl_2 \cdot 2H_2O$.

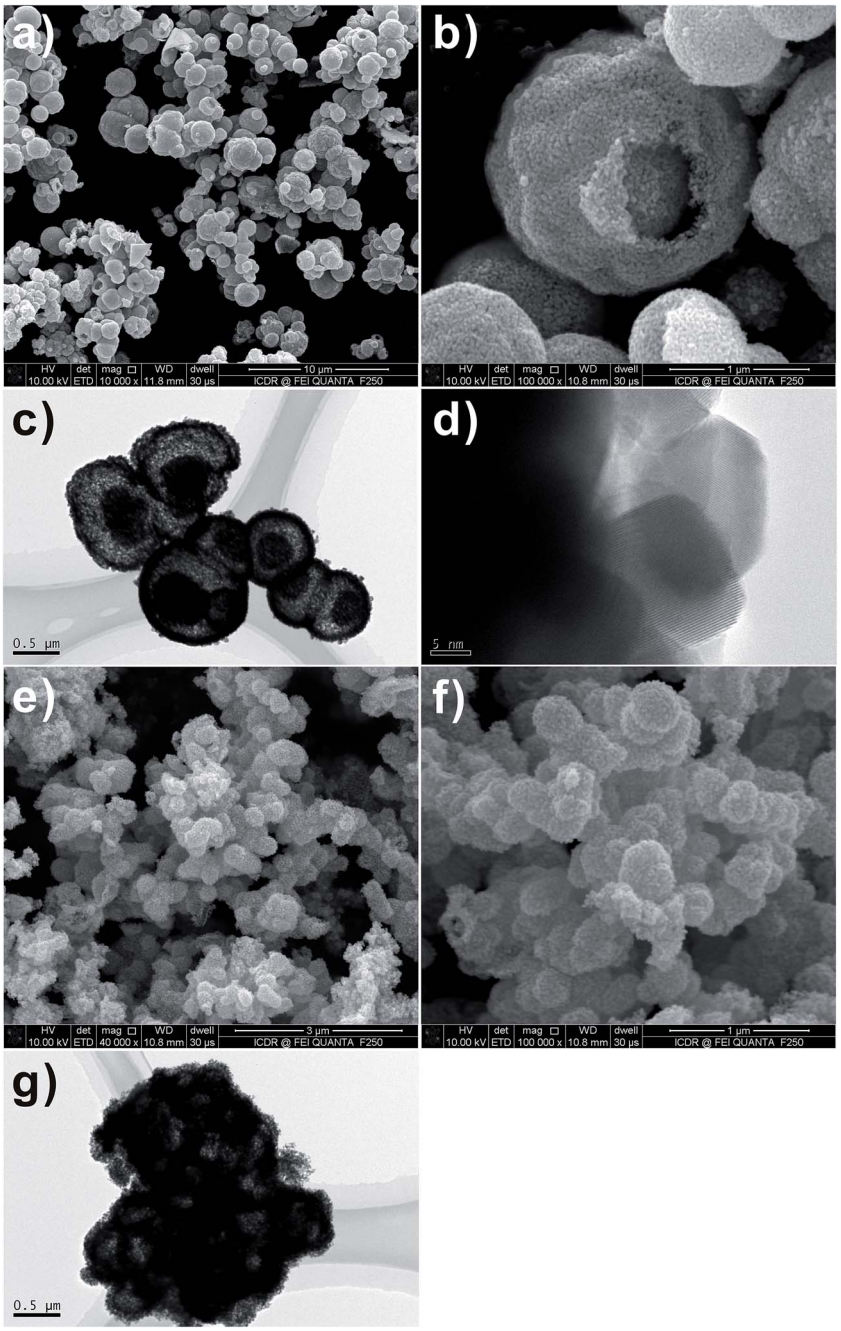

Fig. 5 FESEM and TEM images of SnO_2 samples after calcination at 600 °C for 3 h with 1 : 1 molar ratio of sucrose and metal salt. (a–d) $SnCl_4 \cdot 5H_2O$ and (e–g) $SnCl_2 \cdot 2H_2O$.

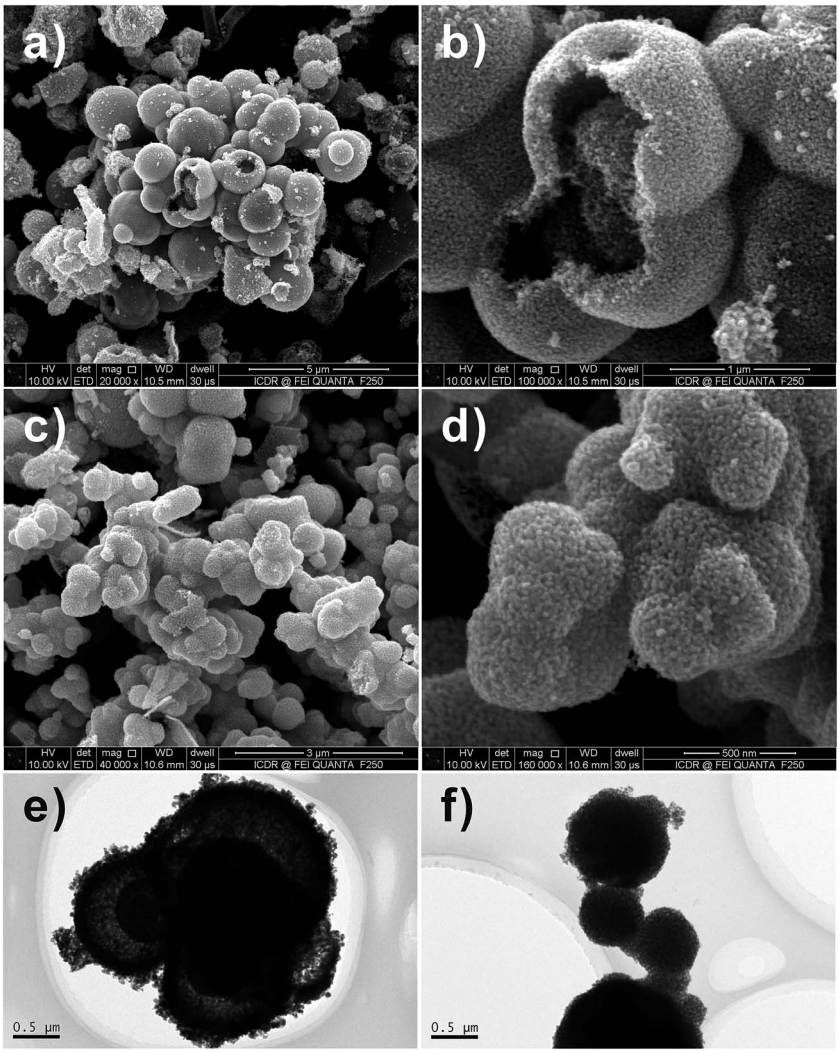

Fig. 6 FESEM and TEM images of SnO_2 samples after calcination at 600 °C for 3 h with (a and b, e) 2 : 1 and (c and d, f) 1 : 2 molar ratio of D-glucose and $SnCl_4 \cdot 5H_2O$.

$SnCl_2$ as the Sn salt source (Fig. 5e and f). Magnified SEM images show that the shell is formed by aggregation of small SnO_2 nanocrystals.

In order to further elucidate the effect of molar ratio of G : M on the morphology of SnO_2 hollow spheres, the SnO_2 products using $SnCl_4$ as Sn salt source, D-glucose as carbon source were characterized by FESEM with different molar ratios of G : M (*i.e.*, 2 : 1 and 1 : 2, respectively). Fig. 6a–d shows the different morphologies of the SnO_2 hollow spheres prepared with different molar ratios of G : M. It is seen that the molar ratio of G : M has important influence on both the size and the morphology of the resulting SnO_2 products. The size of the SnO_2 products decreases with molar ratio of G : M decrease of the system, which could be easily controlled. On the basis of the

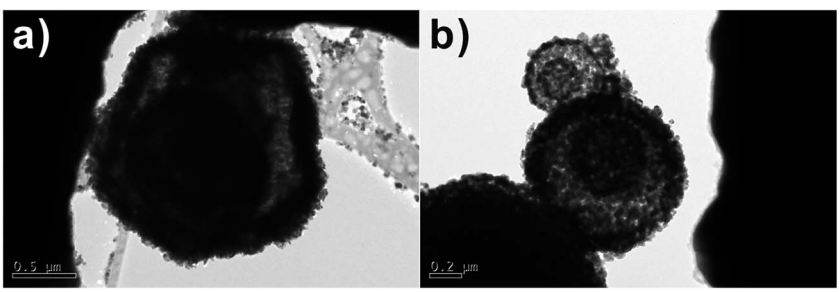

Fig. 7 TEM images of SnO_2 samples after calcination at (a) 700 and (b) 500 °C with 1 : 1 molar ratio of sucrose and $SnCl_4 \cdot 5H_2O$.

morphology analysis results of the SnO_2 products, it is concluded that the SnO_2 products with a large size favor the formation of multi-shelled SnO_2 hollow spheres. We believed that the SnO_2 products with large size could be divided into more regions for the storage of stable Sn species, leading to the formation of shells and solid cores. However, the SnO_2 products prepared with lower molar ratio of G : M could only give rise to relatively small solid SnO_2 particles. Therefore, the molar ratio of G : M in the D-glucose-$SnCl_4$ solution system determines the structure and morphology of the final SnO_2 products.

Fig. 5c, d, g and 6e and f shows the different morphologies of the as-synthesized SnO_2 micro-/nanostructures. As can be seen from the TEM images in the Fig. 5c and 6e, SnO_2 products show similar multi-shelled hollow spheres with hierarchical structures. The outer-shell diameters of these spherical particles are all in the range of 1–2 μm, and the inner spheres have a diameter of 0.5 μm. The TEM images in the Fig. 6e clearly show smaller dark circles inside the hollow spheres, suggesting that the inner SnO_2 spheres still have a hollow structure. Being heat-treated at 600 °C for removal of residual carbon, some multi-shelled SnO_2 hollow spheres had an open hole on their outer shells (Fig. 5 and 6).

The TEM images shown in Fig. 7a and b demonstrate the number of SnO_2 multi-shells increases with temperature, reaching a maximum of 4 multi-shells at 700 °C. Fig. 7a shows that when as-synthesized SnO_2 micro-/nanostructures are heated to 700 °C the inner carbonaceous template gradually separates from the newly formed outer SnO_2 shell, leading to the formation of quadruple-shelled SnO_2 hollow spheres. When the calcination temperature is decreased to 500 °C (Fig. 7b), only double shells with a thin thickness are formed in the SnO_2 samples. As mentioned above, it is expected that the unique multi-shelled structures and increased porosity of the shells could lead to an increase in the electrolyte/SnO_2 contact area, a decrease in the effective diffusion distance for both lithium ion and electrons, and thus better rate capabilities.[18] Second, the void space effectively accommodates the dramatic volume change and alleviates the strain during Li^+-insertion/extraction processes.[19]

Electrochemical properties

Recently, SnO_2 has been a research highlight as a next-generation of anodic material for lithium ion batteries because of its high theoretical specific capacity (~790 mA h g^{-1}). However, it is well known that the main hindrance against practical use of Sn based anode materials in lithium ion batteries is the large volume change during charging–discharging processes which leads to poor cycleability. One possible approach to improve SnO_2 electrochemical performance is to design hollow nanomaterials so as to mitigate the pulverization problem and further enhance structural stability. Inspired by this idea, hollow SnO_2 can provide sufficient space to buffer the volume change during the charging–discharging process and therefore are suggested a cycleable anodic material for lithium ion batteries. The charge–discharge curves of multi-shelled SnO_2 hollow sphere electrodes for the first and the 5th, 10th, 50th and 100th cycle at constant current density of 100 mA g^{-1} are shown in Fig. 8a. The initial discharge and charge capacities are found to be 861 and 422 mA h g^{-1}, respectively. The irreversible capacity loss of 51% can be mainly attributed to the possible irreversible processes, such as electrolyte decomposition and inevitable formation of an SEI layer.[20] Reversible

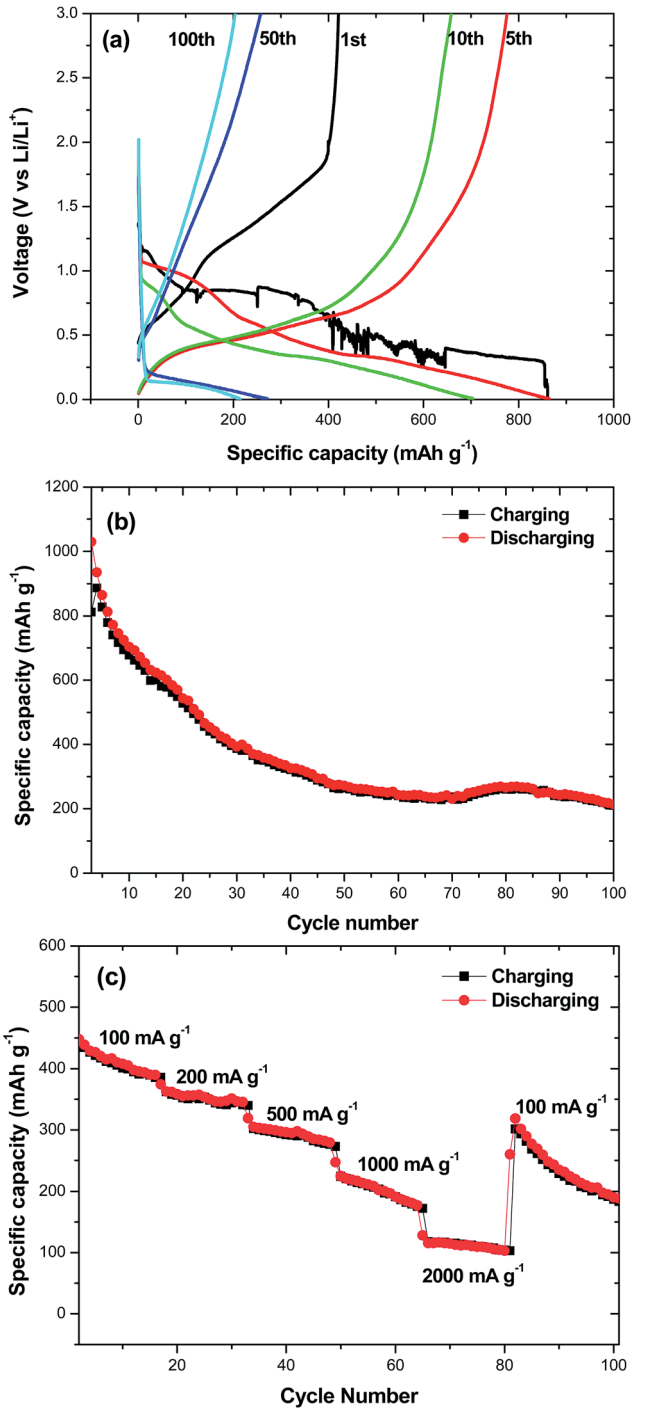

Fig. 8 (a) Charge–discharge curves of the multi-shelled SnO_2 hollow sphere electrode for the 1st, 5th, 10th, 50th, and 100th cycle at current density of 100 mA g^{-1}; (b) the cycling performance of the multi-shelled SnO_2 hollow spheres; (c) charge–discharge curves of the multi-shelled SnO_2 hollow spheres at different current densities.

capacities of 864, 704, 272 and 214 mA h g^{-1} were achieved in the 5th, 10th, 50th and 100th cycle at current density of 100 mA g^{-1}. Fig. 8b shows the cycling performance of the multi-shelled SnO_2 hollow sphere electrode. The charge–discharge capacity of this material remains 214 mA h g^{-1} after 100 cycles, exhibiting a good capacity retention. As the rate capability is also critical for practical applications, we measured charge–discharge curves at different densities for the multi-shelled SnO_2 hollow spheres (Fig. 8c). As can be seen, the average specific capacities of multi-shelled SnO_2 hollow spheres are ~410, 358, 298, 202 and 112 mA h g^{-1} at the current densities of 100, 200, 500, 1000 and 2000 mA g^{-1}, respectively. After the high-rate charge–discharge cycling, a specific capacity as high as ~319 mA h g^{-1} can be restored when the current density is reduced to 100 mA g^{-1}. The above results clearly imply that multi-shelled SnO_2 hollow spheres are relatively tolerant of various charge–discharge currents, which is preferred for high power applications.

Conclusions

In summary, multi-shelled SnO_2 hollow spheres have been successfully prepared through a simple template-free hydrothermal route. The carbon source, Sn salt precursor and molar ratio of G : M play important roles in control of the interior texture of the SnO_2 hollow microspheres. The multi-shelled SnO_2 hollow sphere electrodes exhibit good electrochemical performance as an anode material in lithium ion batteries. The successful synthesis of the multi-shelled SnO_2 hollow nanostructures opens new opportunity for exploitation of metal oxide nanostructures as high-performance anode material for lithium ion batteries.

Acknowledgements

Financial support was provided by National Natural Science Foundation of China (No. 50771082, 51571166, 61505167 and 60776822) and Natural Science Basic Research Plan in Shaanxi Province of China (No. 2015JM5215), Key Project of Baoji University of Arts and Sciences (No. ZK16072), Baoji Engineering Technology Research Center for Ultrafast Optics and New Materials (No. 2015CXNL-1-3). G. Wu thanks the National Natural Science Foundation of China (No. 51407134), China Postdoctoral Science Foundation (No. 2016M590619), and China Postdoctoral Science Special Foundation (No. 2015T81028).

References

1 X. W. Lou, Y. Wang, C. L. Yuan, J. Y. Lee and L. A. Archer, *Adv. Mater.*, 2006, **18**, 2325–2329.
2 Y. J. Hong, M. Y. Son and Y. C. Kang, *Adv. Mater.*, 2013, **25**, 2279–2283.
3 M. M. Titirici, M. Antonietti and A. Thomas, *Chem. Mater.*, 2006, **18**, 3808–3812.
4 J. Qi, X. Y. Lai, J. Y. Wang, H. J. Tang, H. Ren, Y. Yang, Q. Jin, L. J. Zhang, R. B. Yu, G. H. Ma, Z. G. Su, H. J. Zhao and D. Wang, *Chem. Soc. Rev.*, 2015, **44**, 6749–6773.
5 X. Y. Lai, J. E. Halpert and D. Wang, *Energy Environ. Sci.*, 2012, **5**, 5604–5618.
6 H. Ren, J. J. Sun, R. B. Yu, M. Yang, L. Gu, P. Liu, H. J. Zhao, D. Kisailus and D. Wang, *Chem. Sci.*, 2016, **7**, 793–798.
7 J. Y. Wang, N. L. Yang, H. J. Tang, Z. H. Dong, Q. Jin, M. Yang, D. Kisailus, H. J. Zhao, Z. Y. Tang and D. Wang, *Angew. Chem.*, 2013, **125**, 6545–6548.
8 X. Y. Lai, J. Li, B. A. Korgel, Z. H. Dong, Z. M. Li, F. B. Su, J. Du and D. Wang, *Angew. Chem., Int. Ed.*, 2011, **50**, 2738–2741.
9 Z. H. Dong, X. Y. Lai, J. E. Halpert, N. L. Yang, L. X. Yi, J. Zhai, D. Wang, Z. Y. Tang and L. Jiang, *Adv. Mater.*, 2012, **24**, 1046–1049.
10 H. Ren, R. B. Yu, J. Y. Wang, Q. Jin, M. Yang, D. Mao, D. Kisailus, H. J. Zhao and D. Wang, *Nano Lett.*, 2014, **14**, 6679–6684.
11 Z. H. Dong, H. Ren, C. M. Hessel, J. Y. Wang, R. B. Yu, Q. Jin, M. Yang, Z. D. Hu, Y. F. Chen, Z. Y. Tang, H. J. Zhao and D. Wang, *Adv. Mater.*, 2014, **26**, 905–909.
12 G. Q. Zhang and X. W. Lou, *Angew. Chem.*, 2014, **126**, 9187–9190.
13 L. L. Wang, Z. Lou, T. Fei and T. Zhang, *J. Mater. Chem.*, 2011, **21**, 19331–19336.
14 H. X. Yang, J. F. Qian, Z. X. Chen, X. P. Ai and Y. L. Cao, *J. Phys. Chem. C*, 2007, **111**, 14067–14071.
15 J. F. Qian, P. Liu, Y. Xiao, Y. Jiang, Y. L. Cao, X. P. Ai and H. X. Yang, *Adv. Mater.*, 2009, **21**, 3663–3667.
16 H. Wu, G. Wu, Y. Ren, L. Yang, L. Wang and X. Li, *J. Mater. Chem. C*, 2015, **3**, 7677–7690.
17 D. Deng and J. Y. Lee, *Chem. Mater.*, 2008, **20**, 1841–1846.
18 A. Q. Pan, H. B. Wu, L. Yu and X. W. Lou, *Angew. Chem., Int. Ed.*, 2013, **52**, 2226–2230.
19 L. F. Shen, L. Yu, X. Y. Yu, X. G. Zhang and X. W. Lou, *Angew. Chem., Int. Ed.*, 2015, **54**, 1868–1872.
20 H. Guo, Y. P. Wang, W. Wang, L. X. Liu, Y. Y. Guo, X. J. Yang and S. X. Wang, *Part. Part. Syst. Charact.*, 2014, **31**, 374–381.

